Analysis of wheel-rail adhesion redundancy considering the third-body medium on the rail surface

Chun Tian, Gengwei Zhai, Mengling Wu, Jiajun Zhou and Yaojie Li
Institute of Rail Transit, Tongji University, Shanghai, China

Received 31 December 2023
Revised 30 January 2024
Accepted 22 February 2024

Abstract

Purpose – In response to the problem of insufficient traction/braking adhesion force caused by the existence of the third-body medium on the rail surface, this study aims to analyze the utilization of wheel-rail adhesion coefficient under different medium conditions and propose relevant measures for reasonable and optimized utilization of adhesion to ensure the traction/braking performance and operation safety of trains.

Design/methodology/approach – Based on the PLS-160 wheel-rail adhesion simulation test rig, the study investigates the variation patterns of maximum utilized adhesion characteristics on the rail surface under different conditions of small creepage and large slip. Through statistical analysis of multiple sets of experimental data, the statistical distribution patterns of maximum utilized adhesion on the rail surface are obtained, and a method for analyzing wheel-rail adhesion redundancy based on normal distribution is proposed. The study analyzes the utilization of traction/braking adhesion, as well as adhesion redundancy, for different medium under small creepage and large slip conditions. Based on these findings, relevant measures for the reasonable and optimized utilization of adhesion are derived.

Findings – When the third-body medium exists on the rail surface, the train should adopt the low-level service braking to avoid the braking skidding by extending the braking distance. Compared with the current adhesion control strategy of small creepage, adopting appropriate strategies to control the train's adhesion coefficient near the second peak point of the adhesion coefficient-slip ratio curve in large slip can effectively improve the traction/braking adhesion redundancy and the upper limit of adhesion utilization, thereby ensuring the traction/braking performance and operation safety of the train.

Originality/value – Most existing studies focus on the wheel-rail adhesion coefficient values and variation patterns under different medium conditions, without considering whether the rail surface with different medium can provide sufficient traction/braking utilized adhesion coefficient for the train. Therefore, there is a risk of traction overspeeding/braking skidding. This study analyzes whether the rail surface with different medium can provide sufficient traction/braking utilized adhesion coefficient for the train and whether there is redundancy. Based on these findings, relevant measures for the reasonable and optimized utilization of adhesion are derived to further ensure operation safety of the train.

Keywords Wheel-rail adhesion redundancy, PLS-160 wheel-rail adhesion simulation test rig, Normal distribution, Utilized adhesion coefficient

Paper type Research paper

1. Introduction

As an open system, railways are constantly exposed to natural environments, and are often contaminated by third-body medium such as rainwater, air humidity and lubricating oil spilled during the service of trains. This results in a significant reduction in wheel-rail adhesion, which limits the adhesion force that the rail surface can provide. Currently, the traction and braking processes of trains rely on wheel-rail adhesion. When the rail surface cannot provide sufficient adhesion for the train, the wheels may undergo traction

Railway Sciences
Vol. 3 No. 2, 2024
pp. 156-176
Emerald Publishing Limited
e-ISSN: 2755-0915
p-ISSN: 2755-0907
DOI 10.1108/RS-12-2023-0051

overspeeding or braking skidding, which seriously affects the traction and braking performance of the train and poses a significant threat to operation safety of the train. Therefore, the third-body medium on the rail surface creates a sharp contradiction between the adhesion that the rail surface can provide and the actual adhesion utilized by the train, which has become a key issue and challenge that the railway industry is currently focusing on.

The ability of the rail surface to provide sufficient adhesion for the train is usually evaluated using the wheel-rail adhesion redundancy as an indicator. Wheel-rail adhesion redundancy refers to the amount of excess adhesion coefficient provided by the rail surface conditions compared to the actual adhesion coefficient utilized by the train. When the value is greater than 0, it indicates that the rail surface can provide the required adhesion coefficient for the train, otherwise it cannot. By analyzing the wheel-rail adhesion redundancy under different third-body medium conditions based on the designed traction and braking utilization coefficients, it can provide a reference for optimizing the design of the train's traction and braking systems, and is of great significance in ensuring traction and braking performance and operational safety of the train.

Currently, many scholars both domestically and internationally have conducted experimental research on the distribution of adhesion coefficients between wheels and rails under third-body medium conditions such as water and oil. The University of Sheffield Railway Research Institute obtained adhesion coefficients ranging from approximately 0.06 to 0.3 under different flow rate water medium conditions using a dual disc test rig (Trummer, Buckley-Johnstone, Voltr, Meierhofer, Lewis, & Six, 2017; Buckley-Johnstone, Trummer, Voltr, Six, & Lewis, 2020). Chen *et al.* from Railway Technical Research Institute of Japan studied the distribution of adhesion coefficients under different temperature and velocity water medium conditions, ranging from approximately 0.03 to 0.18 (Chen, 2012; Chen & Tanimoto, 2018). Wang *et al.* from Southwest Jiaotong University obtained adhesion coefficients ranging from 0.18 to 0.22 under different axle load water medium conditions using a JD-1 type (1:4 scale) wheel-rail test rig (Wang, Shen, Song, Guo, Liu, & Jin, 2011; Wang, Zhang, Wang, Liu, & Zhu, 2011, Wang *et al.*, 2013; Song, Shen, Wang, Guo, & Liu, 2010). Chang *et al.* from China Academy of Railway Sciences studied the distribution of adhesion coefficients under different water film thickness water medium conditions, ranging from approximately 0.08 to 0.38 using a full-scale wheel-rail test platform (Chang, Chen, Cai, & Wang, 2019). Lewis *et al.* measured that under light oil pollution, wheel-rail adhesion is relatively stable at approximately 0.05 (Lewis, Gallardo-Hernandez, Hilton, & Armitage, 2009). Wang *et al.* measured adhesion coefficients of approximately 0.03 under oil medium conditions (Wang, Shen *et al.*, 2011; Wang, Zhang *et al.*, 2011). Both scholars measured adhesion coefficients lower than 0.1 under oil-water mixed medium conditions. In summary, the adhesion coefficients between wheels and rails under water medium conditions typically range from 0.1 to 0.3, with rare cases below 0.1 or above 0.3. Adhesion coefficients under oil or oil-water mixed medium conditions mostly fall below 0.1. However, the maximum adhesion coefficient currently utilized for traction of domestic Electric Multiple Units (EMU) can reach over 0.18, and the maximum adhesion coefficient utilized for emergency braking can also reach over 0.15. Therefore, in many cases, the presence of third-body medium on the rail surface cannot provide sufficient adhesion for train traction and braking. Currently, most scholars both domestically and internationally conduct experimental research on the adhesion characteristics of wheels and rails under different medium conditions, but no scholar has yet conducted a comparative analysis between rail surface adhesion and train actual utilization adhesion to determine under what conditions trains can ensure traction and braking performance and operational safety. This leads to a lack of clarity regarding whether current adhesion utilization strategies can ensure the operational safety of trains under different rail surface medium conditions. Furthermore, the current traction/braking utilized

adhesion coefficients are mostly controlled near the first peak point of adhesion coefficient-slip ratio curve under the small creepage condition with less than 10% slip ratio (Zhu, Zhou, Kong, Zheng, & Wu, 2020). According to Zhou, Wu, Tian, Yuan, and Chen (2020), adhesion coefficient-slip ratio curve under the large slip condition with a slip ratio exceeding 30% exhibits a "double peak characteristic" of first increasing, then decreasing and finally increasing again. Currently, no scholars have conducted an analysis on whether adhesion coefficient-slip ratio curve under the large slip condition can provide sufficient utilization adhesion coefficients for train. As a result, the current adhesion utilization measures have certain limitations.

In order to clarify whether trains under current adhesion utilization strategies can operate safely under different conditions, achieve reasonable adhesion utilization and improve the upper limit of adhesion utilization, this paper conducted experiments on different rail surface medium, different speeds and different axle loads under small creepage and large slip conditions based on the PLS-160 wheel-rail adhesion simulation test rig. The maximum utilized adhesion characteristics of the rail surface under multiple conditions were obtained. Statistical analysis was conducted on multiple sets of experimental data to obtain the statistical distribution pattern of the maximum utilized adhesion of the rail surface, and a method for analyzing wheel-rail adhesion redundancy based on normal distribution was proposed. The adhesion redundancy of traction and braking under different medium small creepage and large slip conditions was analyzed, and relevant measures for reasonable and optimized adhesion utilization were obtained.

2. Study on maximum utilized adhesion characteristics of rail surface under multiple conditions

To study the maximum utilized adhesion characteristics of the rail surface under third-body medium conditions, the research team has established a circulator wheel-rail adhesion simulation test rig named PLS-160 (Tian, Zhai, Gao, Chen, & Zhou, 2023; Chen, Tian, Huang, & Zhu, 2022, Chen, Tian, Zhou, Zhai, & Yu, 2023), as shown in Figure 1.

The PLS-160 wheel-rail adhesion simulation test rig adopts a fixed track and the rotating wheels design, with a scale ratio of 1:4 and a maximum designed speed of 160 km/h. The test rig is equipped with two wheels, namely a pure rolling wheel and a skidding wheel, which are used to simulate the vehicle speed and axle speed, respectively, to generate the slip ratio. The calculation formula is as follows:

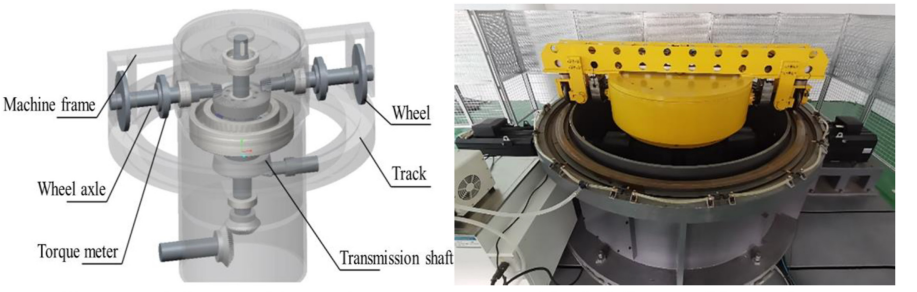

3D structural diagram of the test rig

(a)

Physical diagram of the test rig

(b)

Source(s): Authors own work

Figure 1.
The PLS-160 wheel-rail adhesion simulation test rig

$$s = \frac{(v_c - v_w)}{v_c} \tag{1}$$

In the formula, s represents the slip ratio, v_c [km/h] represents the pure rolling wheel speed (i.e. the vehicle speed), and v_w [km/h] represents the skidding wheel speed (i.e. the axle speed).

The cylinder and the torque meter are installed above the axle of the wheels. By inflating the cylinder to simulate the axle load of the train, the adhesion coefficient at different moments can be calculated based on formula (2):

$$\mu = \frac{T}{R \cdot 1000N \cdot g} \tag{2}$$

In the formula, μ represents the adhesion coefficient at different moments, T [N·m] represents the torque measured at different moments, R [m] represents the radius of the wheel, N [t] represents the simulated train axle load and g represents gravitational acceleration ($g \approx 9.81 \mathrm{m/s^2}$).

By measuring and calculating the slip ratio and adhesion coefficient in real-time during the operation of the test rig, the curve of the adhesion coefficient varying with the slip ratio can be output. The third-body medium spraying device is arranged in a distributed manner along the track, capable of spraying water medium quantitatively. The rail surface can be quantitatively coated with lubricating oil to simulate oil medium pollution. This test rig can simulate small creepage and large slip conditions, more realistically reflecting the maximum utilized adhesion characteristics of the rail surface under dynamic changes in the amount of third-body medium during the skidding process of trains. The PLS-160 wheel-rail adhesion simulation test rig is used to study the small creepage traditional single-peak adhesion coefficient-slip ratio curve and the maximum utilized adhesion characteristics on the rail surface under the large slip conditions.

2.1 Study on the traditional single-peak adhesion coefficient-slip ratio curve of small creepage

The traditional adhesion theory of Kalker, Polach and others suggests that under small creepage conditions, the adhesion coefficient exhibits a characteristic of initially linear increase and subsequent continuous decrease as the slip ratio increases (Kalker, 1982; Polach, 2000, 2005; Piryagin, Polach, & Cole, 2013). To study the maximum utilized adhesion characteristics of the rail surface under small creepage conditions, the PLS-160 wheel-rail adhesion simulation test rig was used to conduct wheel-rail adhesion tests under water, oil and oil-water mixed medium conditions.

2.1.1 Study on the maximum utilized adhesion characteristics of the rail surface under water medium small creepage conditions. Under water medium conditions, the spray flow rate was set to 2L/min, and the water temperature was maintained at room temperature. The target slip ratio was controlled to vary in a sinusoidal pattern from 0 to 0.1 at a period of 12s. 11t axle load was applied to the wheels, and the target speeds were set to 20km/h, 40km/h, 60km/h and 80km/h. The adhesion coefficient-slip ratio curves under water medium small creepage conditions at different running speeds are shown in Figure 2(a). With a target speed of 40km/h, axle loads of 11t, 13t, 15t and 17t were applied to the wheels. The adhesion coefficient-slip ratio curves under water medium small creepage conditions at different axle loads are shown in Figure 2(b).

As shown in Figure 2, under water medium small creepage conditions, the adhesion coefficient exhibits a "single peak" characteristic of initially increasing and subsequently decreasing with the slip ratio, and the peak adhesion coefficient is distributed within the range of 0.2–0.26. With the increase of speed, the adhesion coefficient tends to gradually decrease. With the increase of axle load, the adhesion coefficient slightly decreases, but the difference is small.

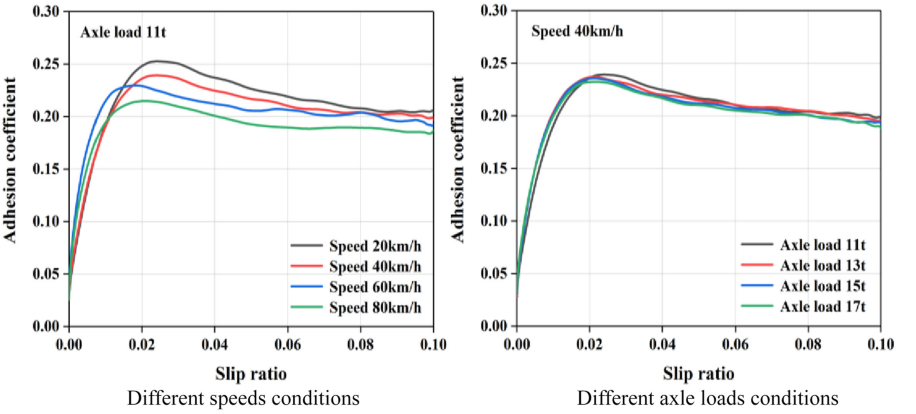

Different speeds conditions (a) Different axle loads conditions (b)

Figure 2.
The adhesion coefficient-slip ratio curves under water medium small creepage conditions

Source(s): Authors own work

2.1.2 Study on the maximum utilized adhesion characteristics of the rail surface under small creepage conditions in other fluid medium. In addition to water medium, oil medium is another common third-body medium on the rail surface. Furthermore, its mixture, oil-water mixed medium, can also have a significant impact on the maximum utilized adhesion characteristics of the rail surface.

Under oil medium conditions, 40ml of type 75W-90 high-speed rail gearbox lubricating oil was uniformly applied to the track. The target slip ratio was controlled to vary in a sinusoidal pattern from 0 to 0.1 at a period of 12s. 11t axle load was applied to the wheels, and the target speeds were set to 20km/h, 40km/h, 60km/h and 80km/h. The adhesion coefficient-slip ratio curves under oil medium small creepage conditions at different running speeds are shown in Figure 3(a). With a target speed of 40km/h, axle loads of 11t, 13t, 15t and 17t were applied to

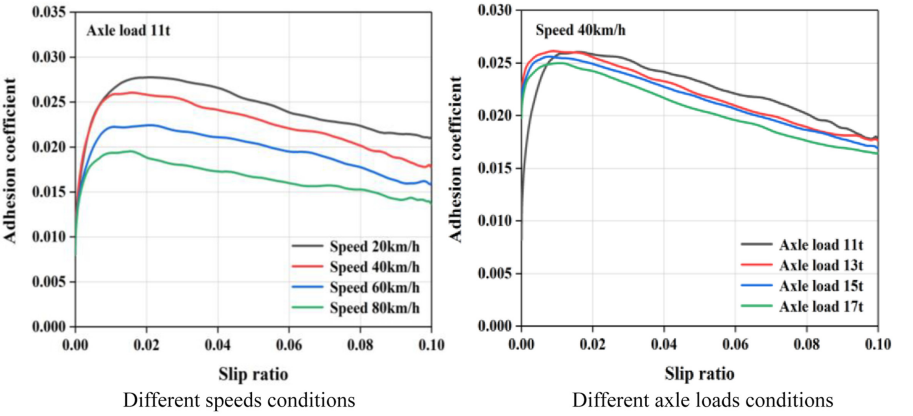

Different speeds conditions (a) Different axle loads conditions (b)

Figure 3.
The adhesion coefficient-slip ratio curves under oil medium small creepage conditions

Source(s): Authors own work

the wheels. The adhesion coefficient-slip ratio curves under oil medium small creepage conditions at different axle loads are shown in Figure 3(b).

As shown in Figure 3, under oil medium small creepage conditions, the adhesion coefficient exhibits a "single peak" characteristic of initially increasing and subsequently decreasing with the slip ratio, and the peak adhesion coefficient is distributed within the range of 0.015–0.03. With the increase of speed, the adhesion coefficient tends to gradually decrease. With the increase of axle load, the adhesion coefficient slightly decreases, but the difference is small.

Under oil-water mixed medium conditions, 40ml of type 75W-90 high-speed rail gearbox lubricating oil was uniformly applied to the track, and the spray device was turned on to spray water medium onto the track at a flow rate of 2L/min, which was stopped after 5s. The target slip ratio was controlled to vary in a sinusoidal pattern from 0 to 0.1 at a period of 12s. 11t axle load was applied to the wheels, and the target speeds were set to 20km/h, 40km/h, 60km/h and 80km/h. The adhesion coefficient-slip ratio curves under oil-water mixed medium small creepage conditions at different running speeds are shown in Figure 4(a). With a target speed of 40km/h, axle loads of 11t, 13t, 15t and 17t were applied to the wheels. The adhesion coefficient-slip ratio curves under oil-water mixed medium small creepage conditions at different axle loads are shown in Figure 4(b).

As shown in Figure 4, under oil-water mixed medium small creepage conditions, the adhesion coefficient exhibits a "single peak" characteristic of initially increasing and subsequently decreasing with the slip ratio, and the peak adhesion coefficient is distributed within the range of 0.03–0.05. With the increase of speed, the adhesion coefficient tends to gradually decrease. With the increase of axle load, the adhesion coefficient slightly decreases, but the difference is small.

2.2 Study on the maximum utilized adhesion characteristics of the rail surface with large slip

Increasingly more experiments have shown that under large slip conditions between the wheel and rail with third-body medium, the adhesion coefficient-slip ratio characteristics exhibit phenomena that are inconsistent with traditional theories (Voltr & Lata, 2015; Bosso, Magelli, & Zampieri, 2019; Chang, Chen, Cai, & Li, 2022, Chang, Chen, Cai, & Wang, 2022). The adhesion coefficient exhibits a trend of first increasing, then decreasing and finally

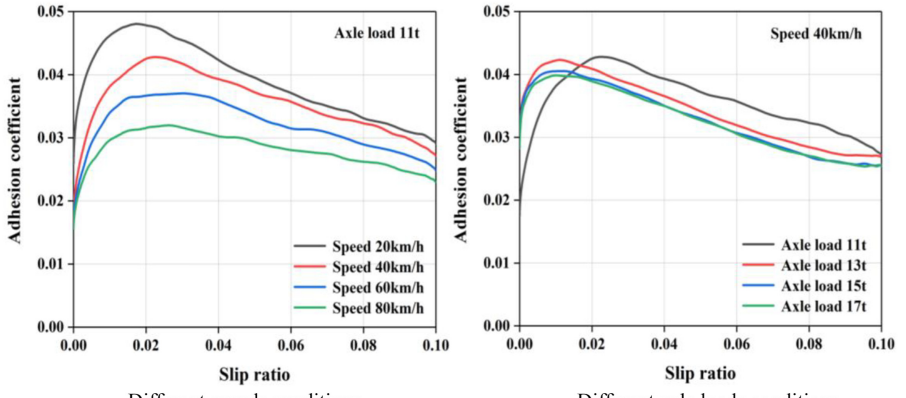

Source(s): Authors own work

Figure 4. The adhesion coefficient-slip ratio curves under oil-water mixed medium small creepage conditions

increasing as the slip ratio increases. To study the maximum utilized adhesion characteristics of the rail surface with large slip, wheel-rail adhesion experiments were conducted under water, oil and oil-water mixed medium conditions using the PLS-160 wheel-rail adhesion simulation test rig.

2.2.1 Study on the maximum utilized adhesion characteristics of the rail surface under water medium large slip conditions. Under water medium conditions, the spray flow rate was set to 2L/min, and the water temperature was maintained at room temperature. The target slip ratio was controlled to vary in a sinusoidal pattern from 0 to 0.3 at a period of 12s. 11t axle load was applied to the wheels, and the target speeds were set to 20km/h, 40km/h, 60km/h and 80km/h. The adhesion coefficient-slip ratio curves under water medium large slip conditions at different running speeds are shown in Figure 5(a). With a target speed of 40km/h, axle loads of 11t, 13t, 15t and 17t were applied to the wheels. The adhesion coefficient-slip ratio curves under water medium large slip conditions at different axle loads are shown in Figure 5(b).

As shown in Figure 5, under water medium large slip conditions, the adhesion coefficient exhibits a "double-peak" characteristic of initially increasing, then decreasing and finally increasing with the slip ratio. The first peak adhesion coefficient is distributed within the range of 0.15–0.25, while the second peak adhesion coefficient is higher than the first peak, indicating an improvement in adhesion. As the speed increases, there is a tendency for the first peak adhesion coefficient to gradually decrease, while the second peak adhesion coefficient gradually increases. With the increase of axle load, the adhesion coefficient slightly decreases, but the difference is small.

2.2.2 Study on the maximum utilized adhesion characteristics of the rail surface under large slip conditions in other fluid medium. Under oil medium conditions, 40ml of type 75W-90 high-speed rail gearbox lubricating oil was uniformly applied to the track. Under oil-water mixed medium conditions, 40ml of type 75W-90 high-speed rail gearbox lubricating oil was uniformly applied to the track, and the spray device was turned on to spray water medium onto the track at a flow rate of 2L/min, which was stopped after 5s. The target slip ratio was controlled to vary in a sinusoidal pattern from 0 to 0.6 at a period of 12s. 11t axle load was applied to the wheels, and the target speeds were set to 60km/h. The adhesion coefficient-slip ratio curves under oil medium and oil-water mixed medium large slip conditions are shown in Figure 6.

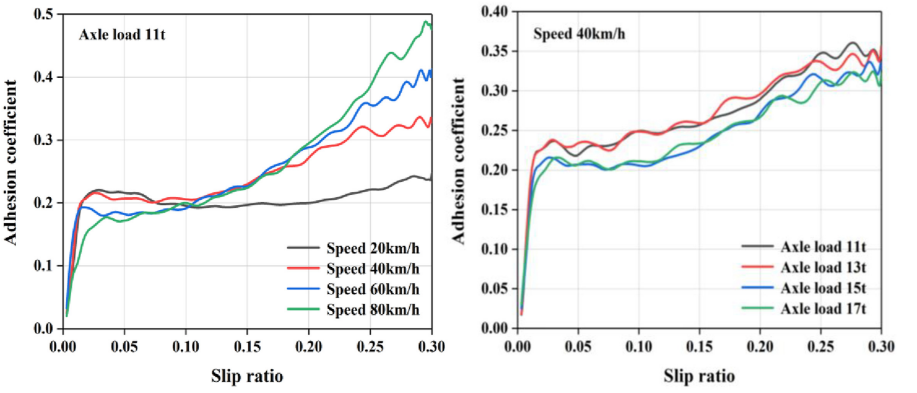

Different speeds conditions (a)

Different axle loads conditions (b)

Figure 5.
The adhesion coefficient-slip ratio curves under water medium large slip conditions

Source(s): Authors own work

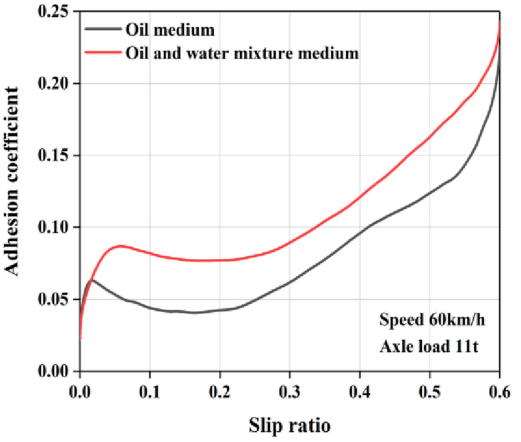

Source(s): Authors own work

Figure 6. The adhesion coefficient-slip ratio curves under oil medium and oil-water mixed medium large slip conditions

As shown in Figure 6, under oil medium and oil-water mixed medium large slip conditions, the adhesion coefficient exhibits a "double-peak" characteristic of initially increasing, then decreasing and finally increasing with the slip ratio. The second peak adhesion coefficient is higher than the first peak, indicating an improvement in adhesion.

2.3 Summary of the maximum utilized adhesion characteristics of the rail surface under multiple conditions

Based on the results of the wheel-rail adhesion tests under various conditions presented in Sections 2.1 and 2.2, the following conclusions can be drawn: Under small creepage conditions, the adhesion coefficient-slip ratio curve exhibits a "single-peak" characteristic, with an initial increase followed by a decrease. The peak adhesion coefficient for the water medium is distributed within the range of 0.2 to 0.26, while the peak values for both the oil and oil-water mixed medium are below 0.1. As the speed increases, the adhesion coefficient tends to decrease, and with an increase in axle load, there is a slight reduction in the adhesion coefficient, but the difference is small. Under large slip conditions, the adhesion coefficient-slip ratio curve demonstrates a "double-peak" characteristic, with an initial increase, subsequent decrease and then another increase. Notably, the second peak of the adhesion coefficient-slip ratio curve has a higher adhesion coefficient compared to the first peak, indicating an improvement in adhesion. Therefore, it can be inferred that the maximum utilized adhesion coefficient of the rail surface is significantly influenced by the third-body medium and speed, while the effect of axle load is relatively minor. However, as the maximum utilized adhesion coefficient of the rail surface is distributed within a range, further research is needed to investigate its distribution patterns.

3. The analysis method of wheel-rail adhesion redundancy based on statistical distribution patterns

As the traction/braking system of the EMU design utilizes a fixed value of adhesion coefficient, and the maximum utilized adhesion coefficient of the rail surface is usually distributed within a range, showing uncertainty. This section studies its statistical distribution patterns. Taking the CRH380A EMU as an example, a wheel-rail adhesion redundancy analysis method based on normal distribution is proposed.

3.1 Study on the statistical distribution pattern of the rail surface maximum utilized adhesion

Repeated experiments were conducted on the PLS-160 wheel-rail adhesion simulation test rig for the various conditions outlined in Section 2 of this paper. Each condition was tested 10 times, resulting in a scatter plot of the maximum utilized adhesion coefficient distribution of the rail surface. Taking the large slip condition with water medium as an example, a sample plot is shown in Figure 7.

The experimental data points were fitted to obtain the black fitted curve in Figure 7. The 200 experimental data points closest to the two peak points of the fitted curve were selected, and the adhesion coefficient values were grouped into 10 groups for statistical analysis. A histogram of the frequency density (frequency/class width) corresponding to the peak points of the adhesion coefficient-slip ratio curve under the water medium large slip condition was obtained.

Based on the statistical method mentioned above, the adhesion coefficient values of the 200 points closest to the peak points of the scatter plot of the maximum utilized adhesion coefficient distribution for different rail surface medium conditions were grouped into 10 groups for statistical analysis. The resulting histograms of the frequency density (frequency/class width) of the peak points' distribution of the adhesion coefficient-slip ratio curve for different medium conditions, along with their probability density fitting curves, are shown in Figure 8.

The adhesion coefficient values of the 200 points closest to the peak points of the scatter plot of the maximum utilized adhesion coefficient distribution for different speed conditions were grouped into 10 groups for statistical analysis. The resulting histograms of the frequency density (frequency/class width) of the peak points' distribution of the adhesion coefficient-slip ratio curve for different speed conditions, along with their probability density fitting curves, are shown in Figure 9.

The adhesion coefficient values of the 200 points closest to the peak points of the scatter plot of the maximum utilized adhesion coefficient distribution for small creepage and large slip conditions were grouped into 10 groups for statistical analysis. The resulting histograms of the frequency density (frequency/class width) of the peak points' distribution of the adhesion coefficient-slip ratio curve for small creepage and large slip conditions, along with their probability density fitting curves, are shown in Figure 10.

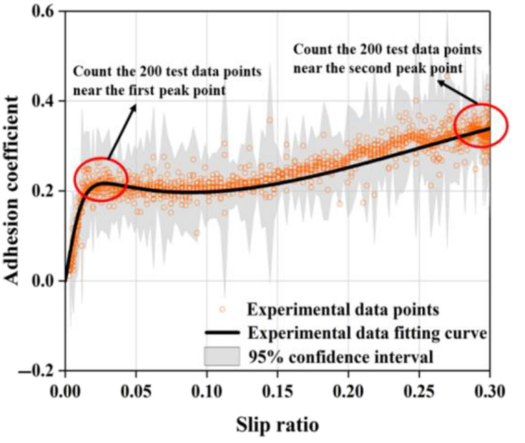

Source(s): Authors own work

Figure 7.
Example scatter plot of the maximum utilized adhesion coefficient distribution under the water medium large slip condition

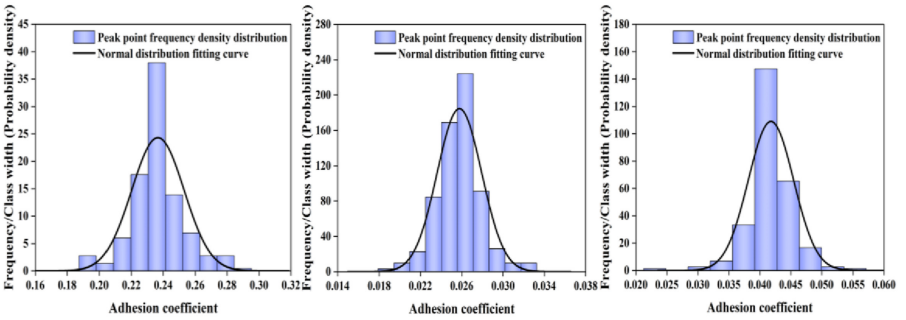

Water medium (a) | Oil medium (b) | Oil-water mixed medium (c)

Source(s): Authors own work

Figure 8. Frequency/probability density plot of the peak points distribution of the adhesion coefficient-slip ratio curve for different medium conditions

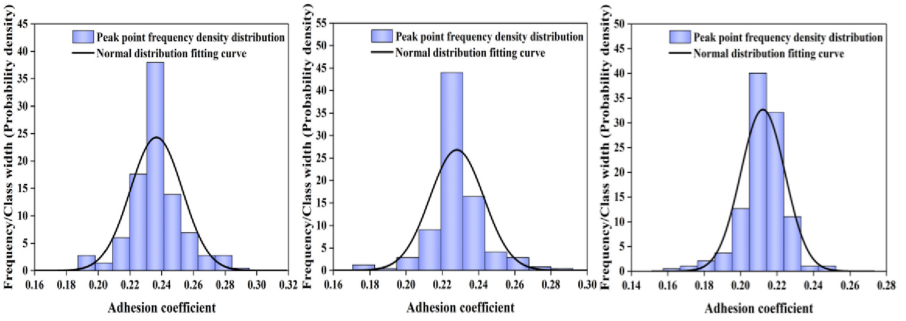

Speed 40km/h (a) | Speed 60km/h (b) | Speed 80km/h (c)

Source(s): Authors own work

Figure 9. Frequency/probability density plot of the peak points distribution of the adhesion coefficient-slip ratio curve for different speed conditions

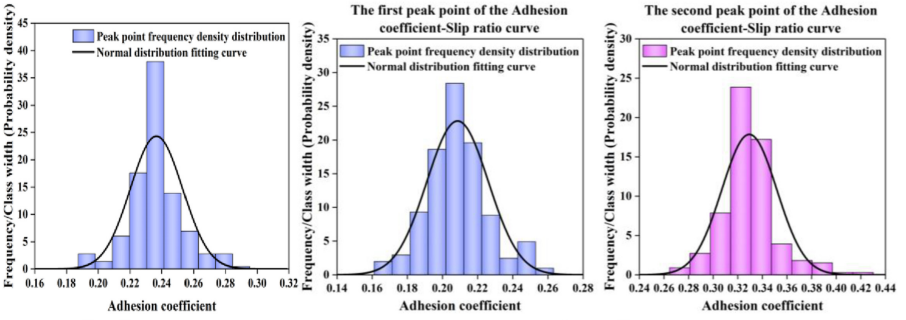

Small creepage (a) | large slip (b)

Source(s): Authors own work

Figure 10. Frequency/probability density plot of the peak points distribution of the adhesion coefficient-slip ratio curve for small creepage and large slip conditions

As shown in Figure 8–10, whether it is under different speeds, axle loads, small creepage or large slip conditions, the distribution histograms of the 200 data points closest to the peak points of the adhesion coefficient-slip ratio curve are centered around the mean adhesion coefficient value, exhibiting a "bell-shaped" distribution with a higher middle and lower sides. Therefore, it is approximately assumed that the maximum utilized adhesion coefficient at the peak points of the adhesion coefficient-slip ratio curve follows a normal distribution. Based on the statistical patterns of the normal distribution, an analysis method for wheel-rail adhesion redundancy can be proposed.

3.2 Analysis method for wheel-rail adhesion redundancy based on the normal distribution

Wheel-rail adhesion redundancy refers to the difference between the maximum utilized adhesion coefficient of the rail surface and the traction/braking utilized adhesion coefficient designed for the train. According to the type of train utilized adhesion coefficient, wheel-rail adhesion redundancy can be divided into traction adhesion redundancy and braking adhesion redundancy. Since the peak points of the rail surface adhesion coefficient-slip ratio curve follow a normal distribution, the analysis of wheel-rail adhesion redundancy needs to consider its distribution probability.

The formula for calculating the traction utilized adhesion coefficient of the train is as follows:

$$\mu_{tuse} = \frac{F_t \cdot 1000}{4 \cdot N \cdot g \cdot \left(P \cdot 1000 \cdot \frac{N_m}{4 \cdot N} \right)} \tag{3}$$

In the formula, μ_{tuse} represents the traction utilized adhesion coefficient for the train, F_t [kN] denotes the total traction force of the train, N is the number of train formations, g stands for gravitational acceleration ($g \approx 9.81 \mathrm{m/s^2}$), P [t] signifies the axle load and N_m represents the total number of powered axles.

The formula for calculating the braking utilized adhesion coefficient of the train is as follows:

$$\mu_{buse} = \frac{a_b}{g} \tag{4}$$

In the formula, μ_{buse} represents the braking utilized adhesion coefficient for the train, and a_b [m/s2] stands for the braking control deceleration.

Based on formulas (3) and (4), as well as the traction characteristic curve and braking control deceleration curve data of the CRH380A EMU, the traction/braking utilized adhesion coefficient of this type of EMU under different speed conditions can be calculated.

According to the distribution pattern of the peak points of the maximum utilized adhesion coefficient of the rail surface under different conditions in Section 3.1, the mean and standard deviation of the 200 points closest to the peak points of the adhesion coefficient-slip ratio curve can be used as the mean and standard deviation of the normal distribution of the peak points. The expressions are as follows:

$$\overline{\mu} = \frac{\sum_{i=1}^{200} \mu_i}{200} \tag{5}$$

In the formula, $\overline{\mu}$ represents the mean adhesion coefficient of the 200 points closest to the peak points of the adhesion coefficient-slip ratio curve, and μ_i (i-1,2,. . .,200) denotes the adhesion coefficient values of different experimental data points.

$$\sigma = \sqrt{\frac{\sum_{i=1}^{200}\left(\mu_i - \overline{\mu}\right)^2}{200}} \tag{6}$$

In the formula, σ represents the adhesion coefficient standard deviation of the 200 points closest to the peak points of the adhesion coefficient-slip ratio curve.

According to formulas (5) and (6), three important intervals of the normal distribution of the adhesion coefficient-slip ratio curve peak points under different conditions can be calculated: the 99.7% confidence interval, the 95% confidence interval and the 68.27% confidence interval. The upper and lower limits of the adhesion coefficient values for these three intervals are $\overline{\mu}\pm3\sigma$, $\overline{\mu}\pm1.96\sigma$, and $\overline{\mu}\pm\sigma$, respectively. The probability that the adhesion coefficient value falls within the 99.7% confidence interval is statistically approximated to be 100%. Based on the mean and standard deviation of the normal distribution of the adhesion coefficient-slip ratio curve peak points under different speed conditions, a curve can be plotted to show the probability interval of the peak points' distribution as it varies with speed.

Taking the adhesion coefficient distribution of the peak points in small creepage conditions with oil-water mixed medium under different speed conditions as an example, a method for analyzing wheel-rail adhesion redundancy based on normal distribution is proposed. The schematic diagram of braking adhesion redundancy analysis for small creepage conditions with oil-water mixed medium is shown in Figure 11.

In Figure 11, the black point-and-line chart represents the normal distribution mean of the peak points of the adhesion coefficient-slip ratio curve under different speed conditions. The three differently colored distribution bands represent the 99.7%, 95% and 68.27% confidence intervals of the peak points of the adhesion coefficient-slip ratio curve under oil-water mixed medium small creepage conditions. The blue and purple point-and-line charts represent the utilized adhesion coefficients for the 2N and 4N levels of the service braking of the CRH380A EMU, respectively. The data points on the utilized adhesion coefficient curve in the figure are divided into three cases (Case 1 ~ Case 3): (1) Utilized adhesion coefficient below the lower limit of the 99.7% confidence interval of the peak normal distribution; (2) Utilized adhesion coefficient within the 99.7% confidence interval of the peak normal distribution; (3) Utilized adhesion coefficient above the upper limit of the 99.7% confidence interval of the peak normal

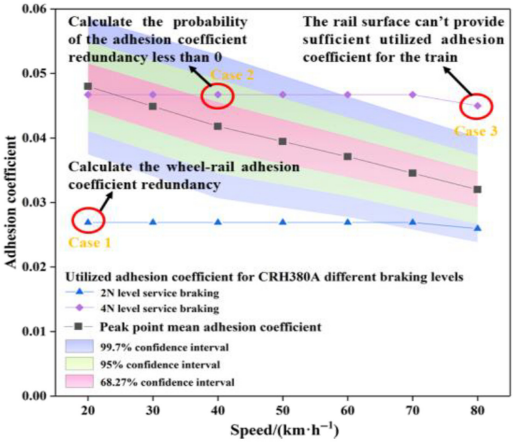

Source(s): Authors own work

Figure 11.
The schematic diagram of braking adhesion redundancy analysis for small creepage conditions with oil-water mixed medium

distribution. Based on the above three cases, a method for analyzing wheel-rail adhesion redundancy based on normal distribution is proposed as follows:

In Case 1, the rail surface can provide sufficient adhesion coefficient for trains with redundancy, and Equation (7) can be used to calculate the adhesion coefficient redundancy. Under this condition, almost no traction overspeeding/braking skidding occurs for trains.

$$\phi = \overline{\mu} - \mu_{buse} \tag{7}$$

In the formula, ϕ represents the wheel-rail adhesion redundancy.

In Case 2, there is a certain probability that the rail surface cannot provide sufficient adhesion coefficient for trains, i.e. the redundancy is less than 0. The probability can be obtained by standardizing the normal distribution using Equation (8) and looking up the standard normal distribution probability table. In this case, there is a certain probability that the train will experience traction overspeeding/braking skidding.

$$z = \frac{\mu_{buse} - \overline{\mu}}{\sigma} \tag{8}$$

In the formula, z represents the standard normal distribution value of the adhesion coefficient.

In Case 3, the rail surface cannot provide sufficient adhesion coefficient for trains, and the wheel-rail adhesion redundancy is almost 100% less than 0, resulting in traction overspeeding/braking skidding for the train.

4. Analysis of wheel-rail adhesion redundancy under different medium conditions

Using the wheel-rail adhesion redundancy analysis method described in Section 3.2, this section calculates and analyzes whether the rail surface can provide sufficient adhesion coefficient for the traction/braking of the CRH380A EMU under various conditions.

4.1 Analysis of wheel-rail adhesion redundancy under small creepage conditions

Based on the utilized adhesion coefficient for traction/braking at different speeds of the CRH380A EMU and the confidence intervals of the normal distribution of the adhesion coefficient-slip ratio curve peak points under water medium small creepage conditions, the analysis diagram of wheel-rail adhesion redundancy under water medium small creepage conditions is obtained as shown in Figure 12.

Using the wheel-rail adhesion redundancy analysis method described in Section 3.2, the traction adhesion redundancy under different speed conditions and the braking adhesion redundancy under different speed and brake level conditions are calculated. The calculated results of wheel-rail adhesion redundancy under water medium small creepage conditions are shown in Tables 1 and 2. The calculation results for Case 1 of wheel-rail adhesion redundancy are represented by Redundancy ϕ, results for Case 2 are represented by probability[%] of ϕ less than 0, and results for Case 3 are represented by insufficient adhesion. The same applies to the following sections.

As shown in Tables 1 and 2, the small creepage conditions with water medium can provide sufficient adhesion coefficient for the traction and braking of the CRH380A EMU with redundancy. As the speed increases, the wheel-rail adhesion redundancy gradually decreases. As the braking level increases, the braking adhesion redundancy also gradually decreases, with a minimum of only 0.0769 redundancies. When the trains designed with higher traction/braking utilized adhesion coefficient are controlled the adhesion near the first peak point of the adhesion coefficient-slip ratio curve under water medium small creepage conditions, there may be no redundancy in the adhesion coefficient, and even a partial

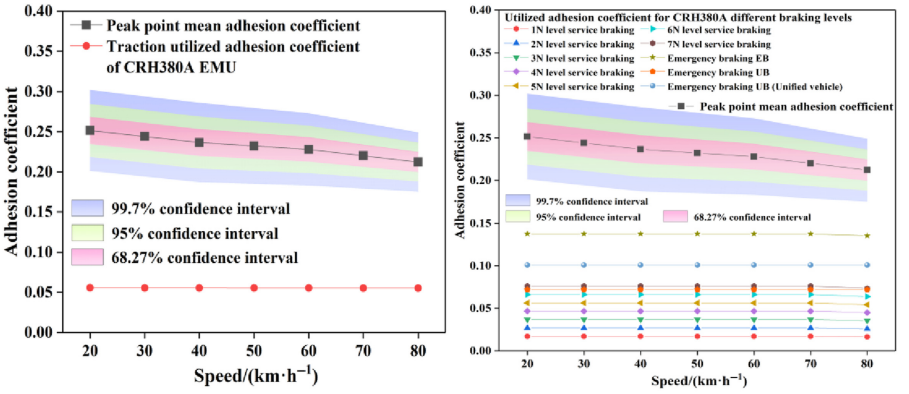

Traction adhesion redundancy (a) Braking adhesion redundancy (b)

Source(s): Authors own work

Figure 12. Analysis diagram of wheel-rail adhesion redundancy under water medium small creepage conditions

Redundancy type	Speed(km/h) 20	30	40	50	60	70	80
Traction adhesion redundancy	Wheel-rail adhesion coefficient redundancy (Case1) 0.1959	0.1885	0.1810	0.1768	0.1726	0.1647	0.1569

Source(s): Authors own work

Table 1. Calculated results of traction adhesion redundancy under water medium small creepage conditions

Braking level	Speed(km/h) 20	30	40	50	60	70	80
Wheel-rail adhesion coefficient redundancy (Case1)							
1N level service braking	0.2346	0.2271	0.2196	0.2153	0.2110	0.2031	0.1958
2N level service braking	0.2247	0.2172	0.2097	0.2054	0.2011	0.1932	0.1862
3N level service braking	0.2148	0.2073	0.1998	0.1955	0.1912	0.1833	0.1767
4N level service braking	0.2049	0.1974	0.1899	0.1856	0.1813	0.1734	0.1672
5N level service braking	0.1952	0.1877	0.1802	0.1759	0.1716	0.1637	0.1579
6N level service braking	0.1853	0.1778	0.1703	0.1660	0.1617	0.1538	0.1483
7N level service braking	0.1754	0.1679	0.1604	0.1561	0.1518	0.1439	0.1387
Emergency braking EB	0.1140	0.1065	0.0990	0.0947	0.0904	0.0825	0.0769
Emergency braking UB	0.1796	0.1721	0.1646	0.1603	0.1560	0.1481	0.1402
Emergency braking UB (Unified vehicle)	0.1507	0.1432	0.1357	0.1314	0.1271	0.1192	0.1113

Source(s): Authors own work

Table 2. Calculated results of braking adhesion redundancy under water medium small creepage conditions

probability of traction overspeeding/braking skidding. Therefore, the train operation controlled near the peak point of the adhesion coefficient-slip ratio curve under water medium small creepage conditions to a certain extent limits the upper limit of traction/braking adhesion utilization.

Based on the utilized adhesion coefficient for traction/braking at different speeds of the CRH380A EMU and the confidence intervals of the normal distribution of the adhesion coefficient-slip ratio curve peak points under oil medium small creepage conditions, the

analysis diagram of wheel-rail adhesion redundancy under oil medium small creepage conditions is obtained as shown in Figure 13.

Using the wheel-rail adhesion redundancy analysis method described in Section 3.2, the traction adhesion redundancy under different speed conditions and the braking adhesion redundancy under different speed and brake level conditions are calculated. The calculated results of wheel-rail adhesion redundancy under oil medium small creepage conditions are shown in Tables 3 and 4.

As shown in Tables 3 and 4, under oil medium small creepage conditions, the CRH380A EMU cannot obtain sufficient adhesion coefficient for traction, as well as for service braking at 3N level and above, and for emergency braking. Additionally, there is a partial probability of insufficient adhesion coefficient for service braking at 1N level above 60 km/h and at 2N level. When the train's adhesion is controlled near the first peak point of the adhesion coefficient-slip ratio curve under oil medium small creepage conditions, the rail surface cannot provide adequate adhesion coefficient for traction/braking of the train. Therefore, during train operation, it is advisable to install some lubricating oil recovery devices on components where lubricating oil may be spilled, or to equip the bogie with rail surface oil stain removal devices. Personnel should also conduct regular inspections of the rail surface oil contamination to ensure, as much as possible, that the rail surface is not contaminated by lubricating oil, thus ensuring operation safety of the train.

Based on the utilized adhesion coefficient for traction/braking at different speeds of the CRH380A EMU and the confidence intervals of the normal distribution of the adhesion coefficient-slip ratio curve peak points under oil-water mixed medium small creepage conditions, the analysis diagram of wheel-rail adhesion redundancy under oil-water mixed medium small creepage conditions is obtained as shown in Figure 14.

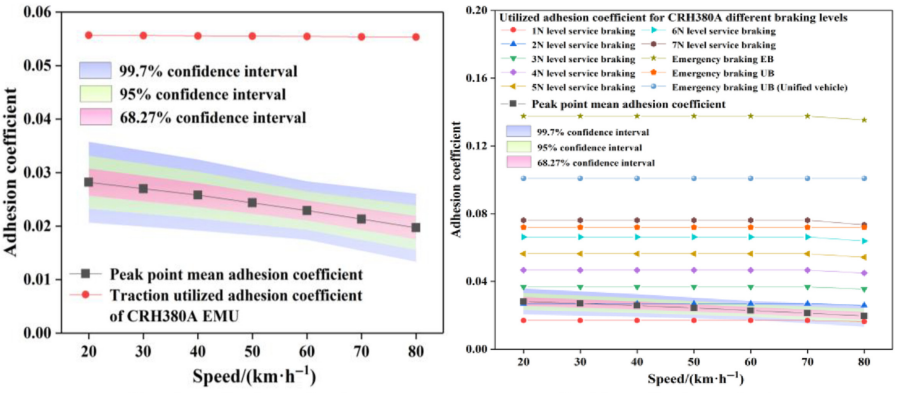

Traction adhesion redundancy (a)

Braking adhesion redundancy (b)

Source(s): Authors own work

Figure 13.
Analysis diagram of wheel-rail adhesion redundancy under oil medium small creepage conditions

Table 3.
Calculated results of traction adhesion redundancy under oil medium small creepage conditions

Redundancy type	Speed(km/h) 20	30	40	50	60	70	80
Traction adhesion redundancy	Insufficient adhesion (Case3)						

Source(s): Authors own work

Using the wheel-rail adhesion redundancy analysis method described in Section 3.2, the traction adhesion redundancy under different speed conditions and the braking adhesion redundancy under different speed and brake level conditions are calculated. The calculated results of wheel-rail adhesion redundancy under oil-water mixed medium small creepage conditions are shown in Tables 5 and 6.

As shown in Tables 5 and 6, when the adhesion of the CRH380A EMU's traction and service braking at 2N level and above, as well as emergency braking, is controlled near the first peak point of the adhesion coefficient-slip ratio curve under oil-water mixed medium small creepage conditions, there is a probability of insufficient adhesion coefficient being utilized, and the

Braking level	Speed(km/h) 20	30	40	50	60	70	80
1N level service braking	Wheel-rail adhesion coefficient redundancy (Case1)					Probability of ϕ less than 0 (Case2)	
	0.0112	0.0100	0.0088	0.0074	0.0059	1.36%	5.82%
2N level service braking	Probability of ϕ less than 0 (Case2)						
	30.15%	48.40%	69.15%	89.97%	98.68%	99.79%	99.86%
3N~7N level service braking	Insufficient adhesion (Case3)						
Emergency braking	Insufficient adhesion (Case3)						

Source(s): Authors own work

Table 4. Calculated results of braking adhesion redundancy under oil medium small creepage conditions

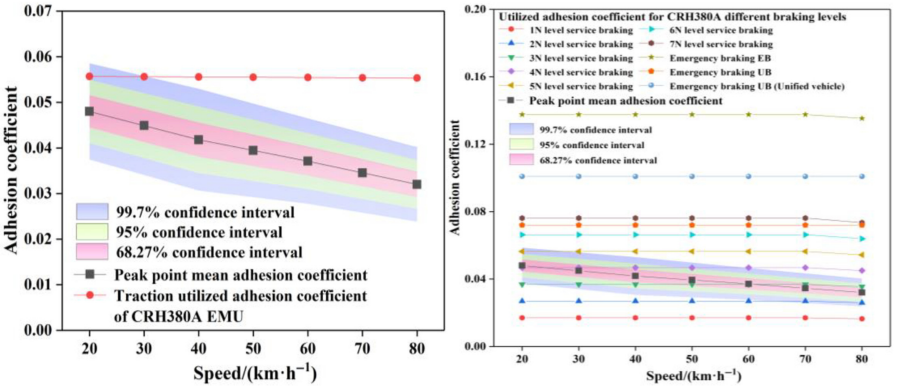

Traction adhesion redundancy (a) Braking adhesion redundancy (b)

Source(s): Authors own work

Figure 14. Analysis diagram of wheel-rail adhesion redundancy under oil-water mixed medium small creepage conditions

Redundancy type	Speed(km/h) 20	30	40	50	60	70	80
Traction adhesion redundancy	Probability of ϕ less than 0 (Case2)		Insufficient adhesion (Case3)				
	98.57%	99.86%					

Source(s): Authors own work

Table 5. Calculated results of traction adhesion redundancy under oil-water mixed medium small creepage conditions

Braking level	Speed(km/h) 20	30	40	50	60	70	80
1N level service braking	Wheel-rail adhesion coefficient redundancy (Case1) 0.0310	0.0279	0.0248	0.0225	0.0201	0.0176	0.0156
2N level service braking	Wheel-rail adhesion coefficient redundancy (Case1) 0.0211	0.0180	0.0149	0.0125	0.0102	Probability of ϕ less than 0 (Case2) 0.41%	1.25%
3N level service braking	Redundancy (Case1) 0.0112	Probability of ϕ less than 0 (Case2) 1.22%	8.85%	21.77%	46.41%	78.23%	90.32%
4N level service braking	Probability of ϕ less than 0 (Case2) 35.57%	69.15%	90.82%	98.38%	Insufficient adhesion (Case3)		
5N level service braking	Probability (Case2) 30.15%	Insufficient adhesion (Case3)					
6N~7N level service braking	Insufficient adhesion (Case3)						
Emergency braking	Insufficient adhesion (Case3)						

Source(s): Authors own work

Table 6.
Calculated results of braking adhesion redundancy under oil-water mixed medium small creepage conditions

probability of insufficient adhesion coefficient for traction and higher-level braking is even greater. Only for 1N level service braking can the adhesion coefficient provided by the rail surface be relatively sufficient, but the redundancy is small. Therefore, it is advisable to avoid oil pollution on the rail surface as much as possible. When there is a third-body medium on the rail surface, it is recommended to use lower-level service braking to avoid the braking skidding through extending the braking distance, thus ensuring operation safety.

4.2 Analysis of wheel-rail adhesion redundancy under large slip conditions

Based on the utilized adhesion coefficient for traction/braking at different speeds of the CRH380A EMU and the confidence intervals of the normal distribution of the adhesion coefficient-slip ratio curve two peak points under water medium large slip conditions, the analysis diagram of wheel-rail adhesion redundancy under water medium large slip conditions is obtained as shown in Figure 15.

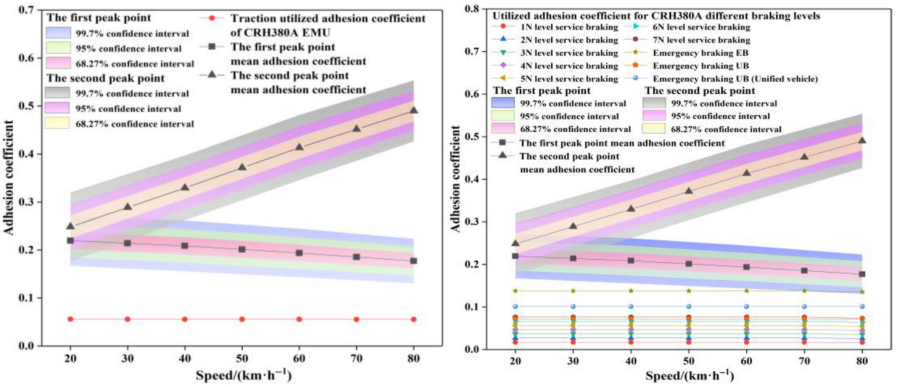

Traction adhesion redundancy (a)

Braking adhesion redundancy (b)

Source(s): Authors own work

Figure 15.
Analysis diagram of wheel-rail adhesion redundancy under water medium large slip conditions

Using the wheel-rail adhesion redundancy analysis method described in Section 3.2, the traction adhesion redundancy under different speed conditions and the braking adhesion redundancy under different speed and brake level conditions are calculated. The calculated results of wheel-rail adhesion redundancy at the two peak points of the adhesion coefficient-slip ratio curve under water medium large slip conditions are shown in Tables 7 and 8.

As shown in Tables 7 and 8, except for the small probability of insufficient adhesion coefficient for CRH380A EMU's emergency braking EB at the first peak point of the adhesion coefficient-slip ratio curve at speeds of 70 km/h and 80 km/h under water medium large slip conditions, the remaining conditions at the first and second peak points can provide sufficient adhesion coefficient for traction and braking of the CRH380A EMU, with redundancy. The adhesion redundancy at the first peak point decreases as the speed increases, while the

Peak point	Speed(km/h) 20	30	40	50	60	70	80
Wheel-rail adhesion coefficient redundancy (Case1)							
The first peak point	0.1637	0.1584	0.1530	0.1457	0.1383	0.1300	0.1217
The second peak point	0.1925	0.2332	0.2738	0.3159	0.3580	0.3962	0.4345

Source(s): Authors own work

Table 7. Calculated results of traction adhesion redundancy under water medium large slip conditions

Braking level	Speed(km/h) 20	30	40	50	60	70	80
The first peak point							
Wheel-rail adhesion coefficient redundancy (Case1)							
1N service	0.2024	0.1970	0.1916	0.1842	0.1767	0.1684	0.1606
2N service	0.1925	0.1871	0.1817	0.1742	0.1668	0.1584	0.1510
3N service	0.1826	0.1772	0.1718	0.1643	0.1569	0.1485	0.1415
4N service	0.1727	0.1673	0.1619	0.1544	0.1470	0.1386	0.1320
5N service	0.1630	0.1576	0.1522	0.1448	0.1373	0.1290	0.1227
6N service	0.1531	0.1477	0.1423	0.1349	0.1274	0.1191	0.1131
7N service	0.1432	0.1378	0.1324	0.1250	0.1175	0.1092	0.1035
Emergency EB	Wheel-rail adhesion coefficient redundancy (Case1)					Probability (Case2)	
	0.0818	0.0764	0.0710	0.0635	0.0561	0.14%	0.33%
Wheel-rail adhesion coefficient redundancy (Case1)							
Emergency UB	0.1474	0.1420	0.1366	0.1291	0.1217	0.1133	0.1050
Emergency UB (Unified vehicle)	0.1185	0.1131	0.1077	0.1002	0.0928	0.0844	0.0761
The second peak point							
Wheel-rail adhesion coefficient redundancy (Case1)							
1N service	0.2312	0.2718	0.3124	0.3544	0.3964	0.4346	0.4734
2N service	0.2213	0.2619	0.3025	0.3445	0.3865	0.4247	0.4638
3N service	0.2114	0.2520	0.2926	0.3346	0.3766	0.4148	0.4543
4N service	0.2015	0.2421	0.2827	0.3247	0.3667	0.4049	0.4448
5N service	0.1918	0.2324	0.2730	0.3150	0.3570	0.3952	0.4355
6N service	0.1819	0.2225	0.2631	0.3051	0.3471	0.3853	0.4259
7N service	0.1720	0.2126	0.2532	0.2952	0.3372	0.3754	0.4163
Emergency EB	0.1106	0.1512	0.1918	0.2338	0.2758	0.3140	0.3545
Emergency UB	0.1762	0.2168	0.2574	0.2994	0.3414	0.3796	0.4178
Emergency UB (Unified vehicle)	0.1473	0.1879	0.2285	0.2705	0.3125	0.3507	0.3889

Source(s): Authors own work

Table 8. Calculated results of braking adhesion redundancy under water medium large slip conditions

adhesion redundancy at the second peak point increases as the speed increases. However, the current maximum utilized adhesion coefficient for traction is 0.18, and the maximum utilized adhesion coefficient for braking is 0.15. Therefore, for other types of EMUs, the first peak point of the adhesion coefficient-slip ratio curve under water medium large slip conditions may not provide sufficient adhesion coefficient for traction/braking. However, the second peak point of the adhesion coefficient-slip ratio curve under water medium large slip conditions can fully provide sufficient adhesion coefficient, with a high redundancy that will further increase as the speed increases.

According to the maximum utilized adhesion characteristics of the rail surface under oil and oil-water mixed medium large slip conditions in Section 2.2.2, the adhesion coefficient at the first peak point is distributed below 0.1, which cannot provide sufficient adhesion condition for some EMUs with higher utilized adhesion coefficient. However, the adhesion coefficient at the second peak point can reach over 0.2, indicating significant adhesion improvement, and can provide sufficient utilized adhesion coefficient for traction/braking of most EMUs.

In summary, regardless of whether the rail surface has water, oil or oil-water mixed medium, by using appropriate strategies to control the utilized adhesion coefficient of the train near the second peak point of the adhesion coefficient-slip ratio curve in large slip conditions, it can effectively increase the adhesion redundancy and utilization upper limit of traction/braking for trains. This has certain reference value for the optimization design of traction/braking systems and ensuring operation safe of the trains.

5. Conclusion

(1) Under water, oil, and oil-water mixed medium small creepage conditions, the adhesion coefficient-slip ratio curves exhibit "single-peak" maximum utilized adhesion characteristics of the rail surface. Water medium is generally able to provide sufficient utilized adhesion coefficient for the CRH380A EMU, while oil and oil-water mixed medium are unable to provide sufficient utilized adhesion coefficient for the CRH380A EMU in most cases.

(2) Under water, oil and oil-water mixed medium large slip conditions, the adhesion coefficient-slip ratio curves exhibit "double-peak" maximum utilized adhesion characteristics of the rail surface. At the first peak point, there is a probability that certain EMUs with higher utilized adhesion coefficient cannot be provided with sufficient adhesion conditions. However, at the second peak point, it is capable of providing sufficient utilized adhesion coefficient for most EMUs.

(3) When the third-body medium exists on the rail surface, the train should adopt the low-level service braking to avoid the braking skidding by extending the braking distance. Compared with the current adhesion control strategy of small creepage, adopting appropriate strategies to control the train's adhesion coefficient near the second peak point of the adhesion coefficient-slip ratio curve in large slip can effectively improve the traction/braking adhesion redundancy and the upper limit of adhesion utilization, thereby ensuring the traction/braking performance and operation safety of the train.

References

Bosso, N., Magelli, M., & Zampieri, N. (2019). Investigation of adhesion recovery phenomenon using a scaled roller-rig. *Vehicle System Dynamics*, *59*(2), 295–312. doi: 10.1080/00423114.2019.1677922.

Buckley-Johnstone, L. E., Trummer, G., Voltr, P., Six, K., & Lewis, R. (2020). Full-scale testing of low adhesion effects with small amounts of water in the wheel/rail interface. *Tribology International*, *141*, 105907. doi: 10.1016/j.triboint.2019.105907.

Chang, C. Y., Chen, B., Cai, Y. W., & Li, G. (2022). Experimental study on large creepage adhesion of wheel/rail braking at 400 km·h-1 (I)-Adhesion characteristics under water medium. *China Railway Science*, *43*(5), 87–93.

Chang, C. Y., Chen, B., Cai, Y. W., & Wang, J. B. (2019). An experimental study of high speed wheel-rail adhesion characteristics in wet condition on full scale roller rig. *Wear*, *440*, 203092. doi: 10.1016/j.wear.2019.203092.

Chang, C. Y., Chen, B., Cai, Y. W., & Wang, J. B. (2022). Experimental study on large creepage adhesion of wheel/rail braking at 400 km·h-1 (I)-Adhesion characteristics under water medium. *China Railway Science*, *43*(2), 96–103.

Chen, H. (2012). Factors that influence the adhesion coefficient between wheel and rail. *Railway Technology Avalanche*, 40, 6.

Chen, H., & Tanimoto, H. (2018). Experimental observation of temperature and surface roughness effects on wheel/rail adhesion in wet conditions. *International Journal of Rail Transportation*, *6*(2), 101–112. doi: 10.1080/23248378.2017.1415772.

Chen, C., Tian, C., Huang, T. X., & Zhu, W. L. (2022). Design and validation of a wheel-rail adhesion simulator in PLS-Circulator. *Journal of Physics: Conference Series*. *2355*(1). doi: 10.1088/1742-6596/2355/1/012038.

Chen, C., Tian, C., Zhou, J. J., Zhai, G. W., & Yu, H. (2023). Development of a new test rig for wheel-rail contact experiments under large slip conditions. *Applied Sciences*, *13*(9), 5320. doi: 10.3390/app13095320.

Kalker, J. J. (1982). A fast algorithm for the simplified theory of rolling contact. *Vehicle System Dynamics*, *11*(1), 1–13. doi: 10.1080/00423118208968684.

Lewis, R., Gallardo-Hernandez, E. A., Hilton, T., & Armitage, T. (2009). Effect of oil and water mixtures on adhesion in the wheel/rail contact. *Proceedings of the Institution of Mechanical Engineers, Part F: Journal of Rail and Rapid Transit*. *223*(3), 275–283. doi: 10.1243/09544097JRRT248.

Piryagin, M., Polach, O., & Cole, C. (2013). Creep force modelling for rail traction vehicles based on the Fastsim algorithm. *Vehicle System Dynamics*, *51*(11), 1765–1783. doi: 10.1080/00423114.2013.826370.

Polach, O. (2000). A fast wheel-rail forces calculation computer code. *Vehicle System Dynamics*, *33*(sup1), 728–739. doi: 10.1080/00423114.1999.12063125.

Polach, O. (2005). Creep forces in simulations of traction vehicles running on adhesion limit. *Wear*, *258*(7-8), 992–1000. doi: 10.1016/j.wear.2004.03.046.

Song, J. H., Shen, P., Wang, W. J., Guo, J., & Liu, Q. Y. (2010). An experimental investigation on the adhesion property of wheel/rail under water conditions. *China Railway Science*, *31*(3), 52–56, DOICNKI:SUN:ZGTK.0.2010-03-011.

Tian, C., Zhai, G., Gao, Y., Chen, C., & Zhou, J. (2023). Study on creepage control for PLS-160 wheel-rail adhesion test rig based on LADRC. *Sensors*, *23*(4), 1792. doi: 10.3390/s23041792.

Trummer, G., Buckley-Johnstone, L. E., Voltr, P., Meierhofer, A., Lewis, R., & Six, K. (2017). Wheel-rail creep force model for predicting water induced low adhesion phenomena. *Tribology International*, *109*, 409–415. doi: 10.1016/j.triboint.2016.12.056.

Voltr, P., & Lata, M. (2015). Transient wheel-rail adhesion characteristics under the cleaning effect of sliding. *Vehicle System Dynamics*, *53*(5), 605–618. doi: 10.1080/00423114.2014.961488.

Wang, W. J., Shen, P., Song, J. H., Guo, J., Liu, Q. Y., & Jin, X. S. (2011). Experimental study on adhesion behavior of wheel/rail under dry and water conditions. *Wear*, *271*(9-10), 2699–2705. doi: 10.1016/j.wear.2011.01.070.

Wang, W. J., Wang, H., Wang, H. Y., Guo, J., Liu, Q. Y., Zhu, M. H., & Jin, X. S. (2013). Sub-scale simulation and measurement of railroad wheel/rail adhesion under dry and wet conditions. *Wear*, *302*(1-2), 1461–1467. doi: 10.1016/j.wear.2012.12.014.

Wang, W. J., Zhang, H. F., Wang, H. Y., Liu, Q. Y., & Zhu, M. H. (2011). Study on the adhesion behavior of wheel/rail under oil, water and sanding conditions. *Wear*, *271*(9-10), 2693–2698. doi: 10.1016/j.wear.2010.12.019.

Zhou, J. J., Wu, M. L., Tian, C., Yuan, Z., & Chen, C. (2020). Experimental investigation on wheel-rail adhesion characteristics under water and large sliding conditions. *Industrial Lubrication and Tribology*, *73*(2), 366–372. doi: 10.1108/ILT-07-2020-0236.

Zhu, W. L., Zhou, J. J., Kong, J. S., Zheng, S. B., & Wu, M. L. (2020). Modeling simulation and testing research of anti-skid control of EMU braking. *Urban Mass Transit*, *12*, 50–55. doi: 10.16037/j.1007-869x.2020.12.010.

Corresponding author
Gengwei Zhai can be contacted at: 2111246@tongji.edu.cn